Interface Fermi States of $LaAlO_3/SrTiO_3$ and Related Heterostructures

C. Cancellieri,* M. L. Reinle-Schmitt, M. Kobayashi, V. N. Strocov, T. Schmitt, and P. R. Willmott
Swiss Light Source, Paul Scherrer Institut, CH-5232 Villigen, Switzerland

S. Gariglio and J.-M. Triscone
DPMC, University of Geneva, 24 Quai Ernest-Ansermet, 1211 Geneva 4, Switzerland
(Received 17 July 2012; published 25 March 2013)

The interfaces of $LaAlO_3/SrTiO_3$ and $(LaAlO_3)_x(SrTiO_3)_{1-x}/SrTiO_3$ heterostructures have been investigated by soft x-ray photoelectron spectroscopy for different layer thicknesses across the insulator-to-metal interface transition. The valence band and Fermi edge were probed using resonant photoemission across the Ti $L_{2,3}$ absorption edge. The presence of a Fermi-edge signal originating from the partially filled Ti $3d$ orbitals is only found in the conducting samples. No Fermi-edge signal could be detected for insulating samples below the critical thickness. Furthermore, the angular dependence of the Fermi intensity allows the determination of the spatial extent of the conducting electron density perpendicular to the interface.

DOI: 10.1103/PhysRevLett.110.137601 PACS numbers: 79.60.Jv, 61.72.S−, 73.20.−r

At the interface between complex oxides, unexpected electronic properties different from those of the constituent bulk materials can arise. A particularly interesting example is the appearance of two-dimensional conductivity at the interface of the band insulators $LaAlO_3$ (LAO) and $SrTiO_3$ (STO) [1–3] at a critical LAO thickness of 4 unit cells (u.c.) [4]. The presence of a critical thickness suggests an intrinsic origin of the metallic state, elegantly explained by the polar catastrophe [5]. According to this scenario, a polar discontinuity at the interface between the polar LAO and nonpolar STO induces electron transfer from the LAO layer into STO Ti $3d$ states (resulting in the formation of Ti^{3+} ions), in response to an increasing divergence of the potential in the LAO layer with its thickness. A recent study on the mixed compound $(LaAlO_3)_x(SrTiO_3)_{1-x}$ (LASTO:x) grown on STO revealed that the critical thickness scales inversely with the LAO content, reaffirming the polar catastrophe as the most likely mechanism responsible for interfacial conductivity [6].

However, there has been some experimental evidence for the presence of conducting electronic states in bare STO [7,8] and below the critical LAO thickness. LAO/STO samples that appear to be insulating from electronic transport measurements show a precursor of electronic reconstruction from second-harmonic-generation experiments [9,10]. In these experiments, an external influence, such as photon-induced doping or sample cleaving, may induce two-dimensional conductivity. Hence, photoemission experiments on buried interfaces measured above and below the critical thickness may allow itinerant electrons in Ti $3d$ states to be directly and unambiguously detected and thereby determine the threshold thickness for electron transfer. More generally, photoemission spectroscopy is a powerful technique which probes the electronic structure of materials and can thus provide a better understanding of their properties.

Hard x-ray measurements of the core levels have already been successfully employed [11–13] to map the spatial extent of the two-dimensional electron gas in LAO/STO perpendicular to the interface, and showed the presence of interfacial Ti^{3+}, also consistent with a recent study using resonant inelastic x-ray scattering on related multilayer structures [14]. A Ti-$3d$-derived density of states should therefore also be seen at the Fermi level (E_F) when electrons are doping STO [15,16]. However, detecting this Ti^{3+} signal at E_F is challenging, due mainly to the buried nature of the interface and the insulating state of the constituent bulk materials. Soft x-ray photoemission measurements performed on LAO/STO heterostructures have highlighted the need to prepare fully oxidized samples, in order to exclude any contributions from oxygen vacancies to the photoemission signal, as well as the importance of selecting the correct photon energy to detect Ti $3d$-states at E_F [17,18]. Ti $2p \rightarrow 3d$ resonant photoemission strongly enhances the photoionization cross section for Ti $3d$-states. In doped STO, the tuning of the photon energy in resonant photoemission experiments was shown to be essential to enhance features associated with a nonzero density of states at E_F [19]. Drera and co-workers [20] found evidence for in-gap states, using Ti $2p \rightarrow 3d$ resonant photoemission spectroscopy, for both conducting and insulating LAO/STO interfaces. Thus, until now, seemingly partly contradictory results on the conducting states at the Fermi level have been reported and no unambiguous picture from photoemission spectroscopic investigations of LAO/STO has yet emerged.

In this Letter, we present clear spectroscopic signatures of Ti^{3+} signal at the Fermi level in fully oxygenated samples of LAO/STO and the related system of mixed LASTO:0.5/STO [6]. Our results show that Ti^{3+}-related charge carriers are present in both systems, but only for conducting samples, and are confined to approximately

one monolayer from the interface. The experiment was performed by varying the photoelectron escape angle and tuning the photon energy ($h\nu$) through the Ti $L_{2,3}$ absorption edge in order to induce resonance enhancement of the photoelectron signal.

LAO and LASTO:x thin films were grown by pulsed laser deposition on (001)-oriented TiO_2-terminated STO substrates at 800 °C at an oxygen pressure of 8×10^{-5} mbar. A KrF excimer laser (248 nm) was used to ablate the sintered targets with a fluence of 0.6 J/cm^2 at a frequency of 1 Hz, leading to a deposition rate of about one unit cell for ~60 laser pulses. After deposition, the oxygen pressure was raised to 0.2 bar and the temperature maintained at 540 ± 10 °C for one hour, in order to ensure full oxidation [21]. Film growth was monitored *in situ* by reflection high-energy electron diffraction. The critical thicknesses required to undergo an insulator-to-metal transition were 4 and 6 u.c. for LAO and LASTO:0.5, respectively, as reported in Refs. [4,6]. The conducting samples of 4.5 LAO and 6 LASTO u.c. showed room-temperature sheet resistances typical of those reported in the literature [6,22]. The insulating samples of LAO/STO and LASTO:0.5/STO were 2.5 and 4 u.c. thick, respectively.

Experiments were performed at the new soft-x-ray angle-resolved photoemission spectroscopy endstation of the Advanced Resonant Spectroscopies (ADRESS) beam line [23] at the Swiss Light Source. This beam line delivers a high photon flux exceeding 10^{13} photons/ sec/0.01% bandwidth, which provides excellent statistics of the interface signal, despite its attenuation as the photoelectrons pass through the film layer. Samples were transferred *ex situ* without any further treatment in vacuum. Charging was avoided by electrically contacting the interfaces using wire bonding to ensure sample grounding.

Measurements were performed using p-polarized light at room temperature. In this case, the atomic thermal motion combined with the relatively small photoelectron wavelength smears the angle-resolved photoemission spectroscopy signal in k space [24]. This suppresses the effects of interface state dispersion, as confirmed by our experimental data, as well as k-dependent variations of the photoemission matrix elements. This simplification enables a straightforward depth-profile analysis. The combined beam line and analyzer energy resolution was set to 150 meV for the valence band spectra and 370 meV for the Ti $2p$ core-level spectra.

We verified the presence of Ti^{3+} by measuring the Ti $2p$ core-level spectra (see Supplemental Material [25]) in a similar manner as that already described by Sing *et al.* [11]. Together with the Ti $2p$ doublet (Ti $2p_{3/2}$ and Ti $2p_{1/2}$) associated with the presence of Ti in the +4 oxidation state, a shoulder at lower binding energy for the conducting samples of 4.5 and 6 u.c. of LAO and LASTO, respectively, indicates the presence of Ti^{3+} spectral weight. This is entirely missing in the insulating interfaces and also consistent with Ref. [11].

The absorption spectrum across the Ti $L_{2,3}$ absorption edge was recorded in total-electron-yield mode for all samples, which agreed precisely with both previously reported experimental data of the Ti^{4+} system [18,26]. The two prominent peaks of the absorption spectrum of the Ti $L_{2,3}$ edge in Fig. 1(a) correspond to the transition from the Ti $2p$ level to the crystal-field split Ti $3d$, t_{2g}, and e_g states. The Ti^{3+} absorption spectrum shown in the same figure, however, is known to be quite different. Both the calculated and experimental Ti^{3+} spectra (recorded for $LaTiO_3$ [18,26]), have an intensity maximum in between the two intense Ti^{4+} L_3 peaks. No change in the spectra and peak positions could be identified with either light polarization, or the type of sample investigated.

Quite distinct behavior between conducting and insulating interfaces was found for the photoemission intensities at E_F taken at different photon energies. Spectral drifts due to charging exhibited by insulating samples were corrected using the valence-band main-peak position as a reference. Moreover, we subtracted the second-harmonic photon contribution which is present in our photon energy range (458–460 eV), due to the Ti $2p$ core level signal excited at $2h\nu$. The intensity map of the whole valence band, recorded by sweeping the photon energy through the Ti $L_{2,3}$ absorption spectrum, is shown in Fig. 1(b). A clear resonance effect is seen for both conducting and insulating samples at 6.8 eV below E_F at the t_{2g} and e_g corresponding photon energies of the Ti L_3 absorption threshold, in agreement with previous studies which show strong hybridization between the oxygen and titanium ions [19,27]. This behavior, typical of a Ti^{4+} system, is observed in all the samples, independent of their conductivity, while any resonance enhancement close to the Fermi energy should be a signature of the presence of Ti^{3+}, that is, metallic behavior. The low-energy binding-energy region close to E_F is enlarged in Fig. 1(c) for a conducting and in Fig. 1(d) for an insulating interface. While no discernible resonance can be observed for the nonconducting sample at any photon energy, the conducting sample has a clear enhancement of the emitted signal, consistent with the Ti $3d$ character of the conduction-band electrons. This is confirmed in Fig. 1(e) where the constant initial state spectra at E_F are shown for the 2.5 and 4.5 u.c. LAO/STO samples. The spectra were obtained from Figs. 1(c) and 1(d), integrating the intensity signal over 1 eV across the Fermi level.

From the above considerations, we selected three photon energies, indicated in Figs. 1(c) and 1(e): 458 (filled black circle) and 460.5 eV (open black circle), corresponding to the prominent peaks of the t_{2g} and e_g Ti states, which are sensitive to Ti^{4+}; and in between, at 459.6 ± 0.25 eV (asterisk) close to the Ti^{3+} absorption maximum [18,26]. This latter value was chosen, as it provided the best enhancement of the photoemitted signal intensity at the Fermi level. The very slight discrepancy with the value of 459.2 eV derived from the absorption spectrum of pure $LaTiO_3$ in Fig. 1(a) is due to the different chemical environment in the two systems and to the different matrix elements in the x-ray absorption and photoemission processes. It is well known that the resonance photoemission process

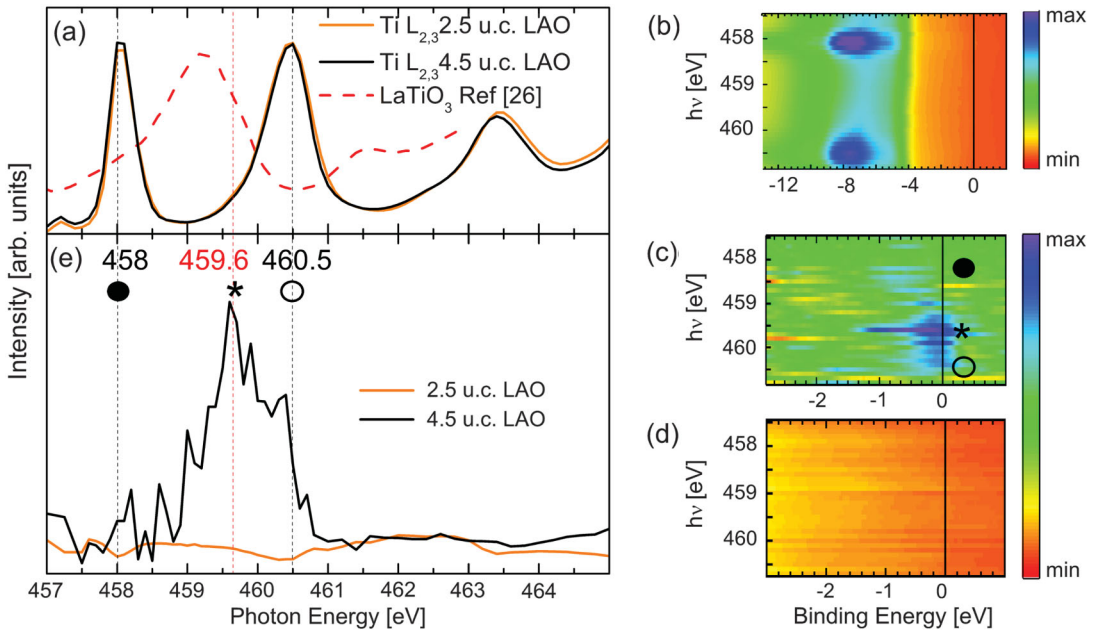

FIG. 1 (color). (a) Ti $L_{2,3}$ absorption-edge spectra taken in total-electron-yield mode for insulating and conducting LAO/STO; in red, adapted from Ref. [26], is the Ti $L_{2,3}$ absorption edge spectrum of $LaTiO_3$, which only contains Ti^{3+} ions. (b) Intensity map of binding energy varying the photon energy ($h\nu$) for conducting LAO/STO. Intensity maps close to the Fermi level of (c) conducting LAO/STO and of (d) insulating LAO/STO. (c) and (d) have the same intensity scale. (e) constant initial state intensity spectra at the Fermi edge for insulating and conducting LAO/STO. The photon energies of 458 and 460.5 eV, indicated with filled and open circles, respectively, correspond to the L_3, t_{2g}, and e_g peaks. The maximum intensity lies at 459.6 eV, indicated with an asterisk.

(autoionization) enhances the Ti 3*d* cross section and signal originating from states in the valence band [19,28,29]. If only Ti^{4+} is present, the Ti 3*d* bands are nominally empty and no resonance enhancement at the Fermi level is expected at any photon energies and in particular at 459.6 eV, while, in contrast, the Ti^{3+} signal should be strongly amplified by resonant autoionization. Hence, any intensity at E_F must be associated with Ti^{3+} ions.

In order to locate the Ti^{3+} states and estimate the thickness of the conducting layer, we tuned the photon energy to correspond to the resonance at E_F and measured the valence-band spectra with varying escape angle θ from 0° (normal emission, bulk sensitive) to 80° [grazing emission, surface sensitive, see inset Fig. 2(a)]. The resonant photoemission spectra for the conducting and insulating samples of LAO and LASTO/STO at different escape angles are shown in Fig. 2. Electronic states at the Fermi energy are evident in conducting samples [Figs. 2(a) and 2(b)]. The intensity at the Fermi level is enhanced through resonant autoionization and varies with the escape angle. Increasing the escape angle results in Fermi-edge signal extinction, as the distance traveled by the electrons from the interface at depth t to the sample surface, $t/\cos\theta$, gradually becomes larger than the photoelectron escape depth. Importantly, as these states are only detectable at the photon energy of 459.6 eV, this indicates that the interface contains Ti^{3+}. As we have already seen in the resonance maps in Fig. 1, the signal at E_F disappears by detuning the photon energy by less than ± 1 eV (see also the Supplemental Material [25]). Importantly, and in contrast to the results of Drera *et al.* [20], the Ti^{3+} signal is not detectable in insulating samples at any of the three employed photon energies [Figs. 1(d) and 1(e), Figs. 2(c) and 2(d), and Supplemental Material [25]]. This discrepancy might be attributable to different sample preparations and postannealing conditions; these can result in the formation of oxygen vacancies, which can contribute to Ti^{3+} in-gap states.

A quantitative analysis of these spectra allowing us to spatially map the conducting layer in the STO requires knowledge of the electron escape depth, λ. We therefore measured the depth profile of the Ti 2*p* core level at $h\nu = 920$ eV, corresponding to the same electronic kinetic energies of ~460 eV used in our resonant measurements of the valence band. From the decay of this signal as a function of angle and knowing the thickness of the film layers, we can extract λ based on the formula:

$$I(\theta) = G(\theta, \phi) \int_0^\infty R(z) e^{-z/\lambda \cos\theta} dz, \qquad (1)$$

where $G(\theta, \phi)$ is a geometrical factor depending on the incident angle and spectrometer acceptance factor (see Supplemental Material [25]), $R(z)$ is the spatial profile of the source of the Ti^{3+} signal (z being the distance from the top surface), and the exponential represents attenuation through the film according to the Beer-Lambert law [30]. The value of the electron escape depth obtained by the fit is $\lambda = 9.5 \pm 1$ Å (see Supplemental Material [25]), in good agreement with National Institute of Standards and Technology database values for this electron kinetic

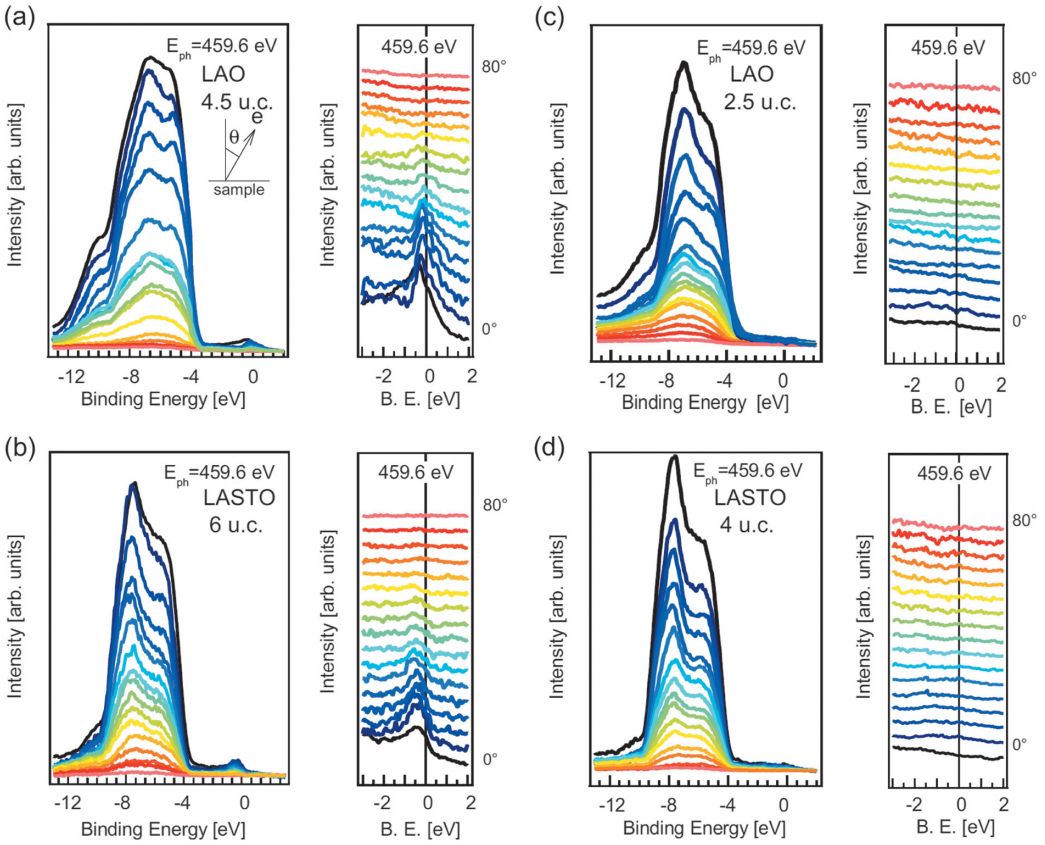

FIG. 2 (color). Photoemission spectra for conducting (a) 4.5 u.c. LAO/STO and (b) 6 u.c. LASTO/STO and for insulating (c) 2.5 u.c. LAO/STO and (d) 4 u.c. LASTO/STO. The color map corresponds to different emission angles θ, indicated on the right of each panel, from 0° (normal emission, black lines) to 80° (grazing emission, pink lines) in 5° steps. The enlarged near-Fermi-edge spectra in (a), (b), (c), and (d) are normalized to the valence band integrated intensity. The x axis in (c) have been corrected for charging shifts in this sample.

energy [31]. We then make the approximation that $R(z)$, the profile of the conducting layer at the interface, is a rectangular function [see Fig. 3(a)]. If we only consider peak-to-background ratios or, in general, when we deal with peak intensity ratios, the $G(\theta, \phi)$ term cancels out. Equation (1) then becomes:

$$I(\theta) = Ae^{-(t+d/2)/\lambda\cos\theta}\sinh\left(\frac{d}{2\lambda\cos\theta}\right), \qquad (2)$$

which, apart from the scaling factor A and the known thickness of the overlayer t, is a function with a single free parameter, d, the thickness of the buried conducting layer. In Figs. 3(b) and 3(c), the integrated E_F peak normalized with the valence band background is plotted as a function of θ. The experimental data are fitted using the expression in Eq. (2); the fits are shown as solid lines in Figs. 3(b) and 3(c). The best fit results are obtained for $d = (1 \pm 0.5)$ u.c. for LAO and $d = (1 \pm 0.3)$ u.c. for LASTO samples. Also shown in Figs. 3(b) and 3(c) are the calculated curves for $d = 5$ u.c. (dashed lines), which deviate significantly from the experimental data, thereby underlining the validity of the fit result. If $R(z)$ is assumed to be exponential or a Gaussian function with a decay length and full width at half maximum, respectively, of 1 u.c., essentially identical results are obtained. The spatial

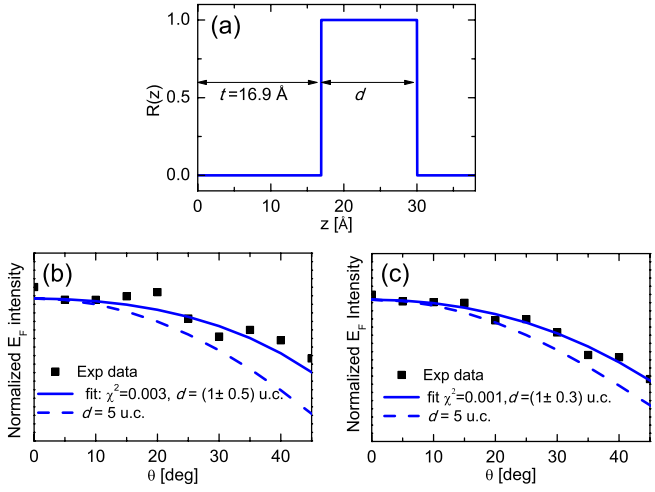

FIG. 3 (color online). (a) Function describing spatially $[R(z)]$ the conducting layer of thickness d at the interface. z is the distance from the film surface. t is the thickness of the film. In this example, $t = 16.9$ Å is the thickness of the 4.5 u.c LAO layer. (b) Normalized Fermi edge integrated intensity as a function of θ for the conducting LAO/STO sample, and (c) the conducting LASTO/STO sample. The best fits, drawn as solid lines in (b) and (c), yield in both cases $d = 1$ u.c.. The dashed lines in (b) and (c) represent the calculated curves for $d = 5$ u.c.

extension of the conducting layer is therefore only one monolayer in the STO substrate.

In conclusion, we have shown clear spectroscopic signatures of the conducting states at the Fermi level for conducting and fully oxidized LAO/STO and LASTO/STO interfaces. These states only become observable if the photon energy is chosen at the resonant absorption energy of the Ti $2p \rightarrow 3d$ transition, demonstrating the presence of electrons in Ti^{3+} states, the latter being also confirmed by Ti $2p$ core-level measurements. In contrast, no signal is detected at the Fermi level using Ti^{4+} resonant photon energies. The variation of the signal of these conducting interface states with the electrons' escape angle unambiguously demonstrates their two-dimensional character and confinement at the interface. The thickness of the conducting layer in STO estimated from the depth profile analysis of the Fermi edge is, for both interfaces of LAO and LASTO, 1 u.c thick on the STO side. The absence of a Ti^{3+} signal for insulating samples below the critical thickness is consistent with the LAO thickness threshold for the onset of conductivity, as predicted by the polar catastrophe scenario.

Support of this work by the Schweizerischer Nationalfonds zur Förderung der wissenschaftlichen Forschung, in particular the National Center of Competence in Research, Materials with Novel Electronic Properties, MaNEP, and by the European Union through the project OxIDes, is gratefully acknowledged. The staff of the Swiss Light Source is gratefully acknowledged. The authors are grateful to C. Wäckerlin for his help in preliminary x-ray photoemission measurements.

*claudia.cancellieri@psi.ch

[1] A. Ohtomo and H. Y. Hwang, Nature (London) **427**, 423 (2004).
[2] N. Reyren, S. Thiel, A. D. Caviglia, L. F. Kourkoutis, G. Hammerl, C. Richter, C. W. Schneider, T. Kopp, A.-S. Retschi, D. Jaccard, M. Gabay, D. A. Muller, J.-M. Triscone, and J. Mannhart, Science **317**, 1196 (2007).
[3] A. D. Caviglia, N. Gariglio, S Reyren, D. Jaccard, T. Schneider, M. Gabay, S. Thiel, G. Hammerl, J. Mannhart, and J.-M. Triscone, Nature (London) **456**, 624 (2008).
[4] S. Thiel, G. Hammerl, A. Schmehl, C. W. Schneider, and J. Mannhart, Science **313**, 1942 (2006).
[5] N. Nakagawa, H. Y. Hwang, and D. A. Muller, Nat. Mater. **5**, 204 (2006).
[6] M. L. Reinle-Schmitt, C. Cancellieri, D. Li, D. Fontaine, M. Medarde, E. Pomjakushina, C. W. Schneider, S. Gariglio, P. Ghosez, J.-M. Triscone, and P. R. Willmott, Nat. Commun. **3**, 932 (2012).
[7] W. Meevasana, P. D. C. King, R. H. He, S.-K. Mo, M. Hashimoto, A. Tamai, P. Songsiriritthigul, F. Baumberger, and Z.-X. Shen, Nat. Mater. **10**, 114 (2011).
[8] A. F. Santander-Syro, O. Copie, T. Kondo, F. Fortuna, S. Pailhes, R. Weht, X. G. Qiu, F. Bertran, A. Nicolaou, A. Taleb-Ibrahimi, P. Le Fevre, G. Herranz, M. Bibes, N. Reyren, Y. Apertet, P. Lecoeur, A. Barthelemy, and M. J. Rozenberg, Nature (London) **469**, 189 (2011).
[9] A. Savoia, D. Paparo, P. Perna, Z. Ristic, M. Salluzzo, F. M. Granozio, U. S. di Uccio, C. Richter, S. Thiel, J. Mannhart, and L. Marrucci, Phys. Rev. B **80**, 075110 (2009).
[10] N. Ogawa, K. Miyano, M. Hosoda, T. Higuchi, C. Bell, Y. Hikita, and H. Y. Hwang, Phys. Rev. B **80**, 081106 (2009).
[11] M. Sing, G. Berner, K. Goß, A. Müller, A. Ruff, A. Wetscherek, S. Thiel, J. Mannhart, S. A. Pauli, C. W. Schneider, P. R. Willmott, M. Gorgoi, F. Schäfers, and R. Claessen, Phys. Rev. Lett. **102**, 176805 (2009).
[12] M. Takizawa, S. Tsuda, T. Susaki, H. Y. Hwang, and A. Fujimori, Phys. Rev. B **84**, 245124 (2011).
[13] Y. Y. Chu, Y. F. Liao, V. T. Tra, J. C. Yang, W. Z. Liu, Y. H. Chu, J. Y. Lin, J. H. Huang, J. Weinen, S. Agrestini, K.-D. Tsuei, and D. J. Huang, Appl. Phys. Lett. **99**, 262101 (2011).
[14] K.-J. Zhou, M. Radovic, J. Schlappa, V. Strocov, R. Frison, J. Mesot, L. Patthey, and T. Schmitt, Phys. Rev. B **83**, 201402 (2011).
[15] T. Yoshida, A. Ino, T. Mizokawa, A. Fujimori, Y. Taguchi, T. Katsufuji, and Y. Tokura, Europhys. Lett. **59**, 258 (2002).
[16] Y. J. Chang, A. Bostwick, Y. S. Kim, K. Horn, and E. Rotenberg, Phys. Rev. B **81**, 235109 (2010).
[17] K. Yoshimatsu, R. Yasuhara, H. Kumigashira, and M. Oshima, Phys. Rev. Lett. **101**, 026802 (2008).
[18] A. Koitzsch, J. Ocker, M. Knupfer, M. C. Dekker, K. Dorr, B. Buchner, and P. Hoffmann, Phys. Rev. B **84**, 245121 (2011).
[19] Y. Ishida, R. Eguchi, M. Matsunami, K. Horiba, M. Taguchi, A. Chainani, Y. Senba, H. Ohashi, H. Ohta, and S. Shin, Phys. Rev. Lett. **100**, 056401 (2008).
[20] G. Drera, F. Banfi, F. F. Canova, P. Borghetti, L. Sangaletti, F. Bondino, E. Magnano, J. Huijben, M. Huijben, G. Rijnders, and D. H. A. Blank, Appl. Phys. Lett. **98**, 052907 (2011).
[21] C. Cancellieri, N. Reyren, S. Gariglio, A. D. Caviglia, A. Fête, and J.-M. Triscone, Europhys. Lett. **91**, 17004 (2010).
[22] S. Gariglio, N. Reyren, A. D. Caviglia, and J.-M. Triscone, J. Phys. Condens. Matter **21**, 164213 (2009).
[23] V. N. Strocov, T. Schmitt, U. Flechsig, T. Schmidt, A. Imhof, Q. Chen, J. Raabe, R. Betemps, D. Zimoch, J. Krempasky, X. Wang, M. Grioni, A. Piazzalunga, and L. Patthey, J. Synchrotron Radiat. **17**, 631 (2010).
[24] L. Plucinski, J. Minár, B. C. Sell, J. Braun, H. Ebert, C. M. Schneider, and C. S. Fadley, Phys. Rev. B **78**, 035108 (2008).
[25] See Supplemental Material at http://link.aps.org/supplemental/10.1103/PhysRevLett.110.137601 for experimental details regarding the spectrometer acceptance factor and determination of the electron escape depth, plus additional spectral data recorded off the Ti^{3+} resonance, and XPS spectra of the Ti $2p$ core electrons.
[26] M. Salluzzo, J. C. Cezar, N. B. Brookes, V. Bisogni, G. M. De Luca, C. Richter, S. Thiel, J. Mannhart, M. Huijben, A. Brinkman, G. Rijnders, and G. Ghiringhelli, Phys. Rev. Lett. **102**, 166804 (2009).
[27] Z. Zhang, S.-P. Jeng, and V. E. Henrich, Phys. Rev. B **43**, 12 004 (1991).
[28] L. C. Davis, Jpn. J. Appl. Phys. **59**, R25 (1986).
[29] M. Takizawa, H. Wadati, K. Tanaka, M. Hashimoto, T. Yoshida, A. Fujimori, A. Chikamatsu, H. Kumigashira, M. Oshima, K. Shibuya, T. Mihara, T. Ohnishi, M. Lippmaa, M. Kawasaki, H. Koinuma, S. Okamoto, and A. J. Millis, Phys. Rev. Lett. **97**, 057601 (2006).
[30] R. W. Paynter, J. Electron Spectrosc. Relat. Phenom. **169**, 1 (2009).
[31] NIST Standard Reference Database 82, version 1.3.